DEFORMATION ANALYSIS OF A BORED TUNNEL BY MEANS OF TERRESTRIAL LASER SCANNING

Rinske van Gosliga[1], **Roderik Lindenbergh**[2] **and Norbert Pfeifer**[3]

1: Gemeentewerken Rotterdam; r.vangosliga@gw.rotterdam.nl
2: Delft University of Technology, Delft Institute of Earth Observation and Space Systems; r.c.lindenbergh@tudelft.nl
3: alpS Centre for Natural Hazard Management, Innsbruck; norbert.pfeifer@uibk.ac.at

KEY WORDS: Terrestrial laser scanning, point cloud modeling, tunnel deformation detection

ABSTRACT:

A procedure is developed, implemented and tested to detect deformations in a bored tunnel. Deformations can occur after construction of the tunnel is finished, i.e. between two measurement epochs, but also deformations of the completed tunnel with respect to the design model are considered. For this procedure first the tunnel model is fitted to a point cloud consisting of several registered terrestrial laser scans using a linearized iterative least squares approach. This results in approximately optimal values for the tunnel model. Then deformations with respect to this tunnel model or between epochs are determined by means of a statistical testing procedure. Results performed together with the municipality of Rotterdam show that the studied tunnel is not so much ovalizing as a whole after construction, as was expected, but rather that single tunnel segments show different deviation patterns.

1. INTRODUCTION

In Rotterdam a new means of public transport to The Hague is under construction, named RandstadRail. For this new light rail connection, a tunnel is to be bored in the north of Rotterdam. The department Landmeten en Vastgoedinformatie (LV) of Gemeentewerken Rotterdam (GW) performs measurements for the construction of this tunnel. Besides the conventional tachymetric measurements, e.g. (Kontogianni and Stiros, 2003), and leveling, LV wants to use terrestrial laser scanning for the determination of tunnel deformations. With tachymetry small deformations can be detected with high precision but only for a few selected positions due to the largely manual measurement process. Laser scanning, on the other hand, is best suited for measurements over areas, but offers less precision. The hypothesis is that the large number of points measured can compensate for the reduced precision and allows studying the deformation over the complete tunnel surface. Little knowledge exists about the possibilities of deformation analysis with terrestrial laser scanning, (Tsakiri et al., 2006), therefore the research described in this report has been performed. Tunnel measurements with terrestrial laser scanning is also discussed in (Schulz and Ingensand, 2004). Tunnel surface observations can also be performed by photogrammetric means, e.g. using the system (Dibit, 2006), or combined with laser scanning (Paar et al., 2005). Using laser scanning alone has the potential of allowing fast measurements, covering the entire tunnel surface, eventually extracting deformations, all without the need for elaborated calibration tasks.

An inventory of existing laser scanners (Lemmens, 2004; POB, 2006) shows that a phase-based scanner is most efficient for measurements in the RandstadRail bore tunnel. This type of scanner measures fast, i.e. with measurement rates of more than 100000 points per second. Phase based scanners also exhibit better precisions compared to scanners measuring range based on pulse round trip time. However, measurement range is comparatively short, typically up to 50m. The high measurement speed results in a high point density. The scans were obtained from fixed scan locations. Alternatively the scanning can be performed by a moving scanner (Blug et al., 2005).

The method that is set up for the *deformation analysis* estimates an analytical model of the object. For a bored tunnel this is typically a circular cylinder or a more complex model (e.g., an elliptic cylinder) that follows the ideal construction plan. The parameters of the model are estimated by model fitting using least squares adjustment. The differences between the scan data and the model are an indication for the deformation of the tunnel with respect to the construction plan. Besides, *scan data collected at two different epochs* are compared to show changes in time. The scan data is partitioned into cells with the raster laid out over the object. For both scans the same partitioning is used. For each cell a grid point is determined by adjustment of the scan data using a simple model, which is a local approximation of the overall analytical model. Using a stability test it is tested whether two corresponding grid points have been stable in time. A *measurement setup* for deformation detection with laser scanning is made and a test measurement is performed in the 2^{nd} Heinenoordtunnel. Then a method is drawn up for the deformation analysis and this is put into practice on the collected data. Data is processed by software belonging to the laser scanner and by a computational program written in Matlab.

In Sec. 2 the methodology is presented, comprising cylinder fitting and deformation analysis. Sec. 3 describes the data acquisition and processing. In the last section conclusions are drawn for both the analysis of the Heinenoordtunnel and the methodology used, while future work for improving the process is identified.

2. METHODOLOGY

2.1 Cylinder fitting

Observations in scanner coordinates The original measurements of a terrestrial laser scanning device are angles and ranges, also termed distances. For each three dimensional object point $\mathbf{p_i^\circ}$ the angles in the spherical coordinate system α_i and β_i and the distance d_i are measured. Therefore

$$\mathbf{p_i^\circ} = d_i(\cos\alpha_i \cos\beta_i, \sin\alpha_i \cos\beta_i, \sin\beta_i)^\top \quad (1)$$

While the measurement precision m_α and m_β of the angles are only depending on the device itself, the distance precision m_d also depends on the material properties of the reflecting surface, its extent, and the incidence angle of the laser ray on the surface. The measurements are performed in the spherical coordinate system local to the scanner, but a translation $\mathbf{t}$ and a rotation $\mathbf{R}$ is applied to the points in the registration process. In the following it is assumed that a set of object or observation points $\mathbf{p_i} = \mathbf{t} + \mathbf{R} \cdot \mathbf{p_i^\circ}$ is given in a common spherical coordinate system.

Cylinder parameterization Cylinders in 3D have five degrees of freedom, one for the radius r and four for the axis, which can be divided into two parameters for the direction and two for the position. Let $\bar{\mathbf{p}}$ be the barycenter of the observation points $\mathbf{p_i}$, or any other convenient fixed point in the vicinity of the measured points. With the unit vector of the cylinder axis direction

$$\mathbf{a} \quad = \quad (\cos\lambda\cos\phi, \sin\lambda\cos\phi, \sin\phi)^\top, \tag{2}$$

the position of the cylinder axis is fixed by specifying the point on the cylinder axis most close to $\bar{\mathbf{p}}$ as

$$\mathbf{c} \quad = \quad \bar{\mathbf{p}} + u \cdot \mathbf{n_u} + v \cdot \mathbf{n_v} \tag{3}$$

in an orthonormal basis $(\mathbf{a}, \mathbf{n_u}, \mathbf{n_v})$ of $\mathbb{R}^3$, where $\mathbf{n_u}$ and $\mathbf{n_v}$ are defined by e.g.

$$\begin{aligned} \mathbf{n_u} &= (-\sin\lambda\cos\phi, \cos\lambda\cos\phi, 0)^\top \\ \mathbf{n_v} &= (-\cos\lambda\sin\phi, -\sin\lambda\sin\phi, \cos\phi)^\top. \end{aligned} \tag{4}$$

The five cylinder parameters are then r, λ, ϕ, u, v. This parameterization is similar to the one proposed in (Lukács et al., 1997).

Observation equations. In least squares adjustment (Teunissen, 2000a) the measurement errors in the original observations are minimized. In this case these errors are $e_{\alpha,i}$, $e_{\beta,i}$, and $e_{r,i}$. In order to formulate this minimization problem, the observations are expressed as functions of the parameters. Therefore, the unknown location of the point $\mathbf{p_i}$ on the cylinder has to be introduced as parameter in the adjustment, too. Using cylindrical coordinates, two numbers (y, θ) are used for specifying a location, y, along the axis and a rotation, θ, around it. A point $\mathbf{q}$ on the cylinder skin is expressed as

$$\mathbf{q} \quad = \quad \mathbf{c} + (y \cdot \mathbf{a} + r\cos\theta \cdot \mathbf{n_u} + r\sin\theta \cdot \mathbf{n_v}) \tag{5}$$

Each observation (r_i, α_i, β_i) gives the following contribution to the observation equations:

$$\begin{pmatrix} r_i + e_{r,i} \\ \alpha_i + e_{\alpha,i} \\ \beta_i + e_{\beta,i} \end{pmatrix} \;=\; f(\mathbf{x}), \text{ with } \mathbf{x} = (r, \phi, \lambda, u, v, y_i, \theta_i) \tag{6}$$

Here $f : \mathbb{R}^7 \rightarrow \mathbb{R}^3$ describes the non-linear cylindrical model in the parameterization of above. For each object point consisting of three measurements two parameters are introduced, leading to a redundancy of $n - 5$, where n is the number of measured points. The advantage of the above formulas is that the original observations are used, allowing proper error modeling. These equations can be simplified if instead of the original observations (r_i, α_i, β_i) the Cartesian coordinates (x_i, y_i, z_i) of $\mathbf{p_i}$ are used. In that case however, the covariance matrix of each point becomes a full matrix, whereas it is only a diagonal matrix when using the original observations (assuming independent measurements). The disadvantage of the above equations is that with laser scanning millions of points are measured which leads to a normal equation system with a dimension of two times the number of points plus five.

Reducing the observation space. In order to keep the number of parameters small, a simpler adjustment is performed. Not the measurement errors, but the distances of the measured points to the cylinder are minimized. For this end the cylinder is defined as zero set of

$$e(\mathbf{p}) \quad = \quad \|(\mathbf{p} - \mathbf{c}) \times \mathbf{a}\| - r, \tag{7}$$

see also Fig. 1. Here $\|\cdot\|$ denotes vector length and $\times$ the vector cross product. The length of the vector $(\mathbf{p}-\mathbf{c}) \times \mathbf{a}$ is equal to the area of the parallelogram spanned by vectors $\mathbf{a}$ and $\mathbf{p} - \mathbf{c}$, which is in turn equal to the rectangle with the same base and height. Using $\mathbf{a}$, which is a unit vector, as base, this area becomes equal to the height (only differing in the units meter and m^2, respectively). It is concluded that the length $\|(\mathbf{p} - \mathbf{c}) \times \mathbf{a}\|$ equals the distance of $\mathbf{p}$ to the cylinder axis. For a point on the cylinder skin this value is exactly the radius r. The value $e(\mathbf{p})$ is not only an algebraic distance measure, as it is in fact the value of an implicit function, but it specifies the Euclidean distance of $\mathbf{p}$ to the cylinder as well. This means that $e(\mathbf{p})$ is the length of the vector from $\mathbf{p}$ to its orthogonal projection onto the cylinder.

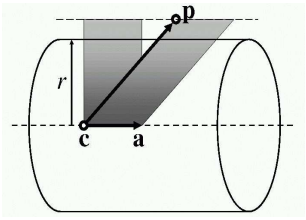

Figure 1. Cylinder definition with vector product.

Without measurement errors this distance would be zero always, but in a real situation only its expectancy becomes zero and this distance is written as $0+e_i$. The "observation" equation therefore takes the following form

$$0 + e_i \quad = \quad \|(\mathbf{p_i} - \mathbf{c}) \times \mathbf{a}\| - r \tag{8}$$

In this form only the five parameters (r, λ, ϕ, u, v) describing the cylinder remain to be estimated. A further simplification is reached by over-parameterizing the cylinder by specifying $\mathbf{a} = (a_x, a_y, a_z)$ and $\mathbf{c} = (c_x, c_y, c_z)$ and introducing two additional constraints (or highly weighted observation equations) of the following form:

$$1 + e_a \;=\; \|\mathbf{a}\| \qquad \text{and} \qquad 0 + e_y \;=\; c_y \tag{9}$$

The first equation specifies that the axis vector must be a unit vector and the second equation fixes one coordinate of the point on the cylinder axis. The y-coordinate is chosen because the cylinder axis is roughly aligned with the y-axis of the coordinate system.

Reduction justification. The different methods presented above (adjusting the observations, minimizing the orthogonal distances, and minimizing the orthogonal distances with over-parameterization) were compared numerically using up to 10000 points and an identity matrix as weight matrix. For the examples encountered in this tunnel study no significant difference could be found, i.e. the results are equal up to the 7th digit. While it appears intuitively that minimizing the orthogonal distances of the points to the cylinder surface on the one hand, and minimizing the measurement errors on the other hand, should lead to the same results, the authors note that this is not proven within this paper.

Initial guess of the tunnel parameters. For performing the adjustment the above observation equations have to be linearized, (Teunissen, 2000a). For initialization of the linearization algorithm approximate values for the cylinder parameters have to be computed first. For this purpose normal vectors $\mathbf{n_i}$ in the measured points $\mathbf{p_i}$ are estimated by fitting that plane to the e.g. 10 nearest neighbors of each $\mathbf{p_i}$, that minimizes the orthogonal distances of the points in the least square sense. The normal vectors of a cylinder describe a great circle on the unit sphere with the carrier plane orthogonal to the cylinder axis. The direction

of the cylinder axis is therefore approximated by fitting a plane through the normal vectors $\mathbf{n_i}$ (i.e. the points on the unit sphere). To ensure that a great circle and not a small circle is obtained the origin should also be included in this fitting procedure with a weight equal to the number of normal vectors. The normal vector again of this plane gives a good first approximation for the cylinder axis $\mathbf{a}$. For the examples in this study taking the barycentre of the observation points $\mathbf{p_i}$ as approximate value of $\mathbf{c}$ proofed to be sufficient in all cases. An approximate tunnel radius r was known from the tunnel design to be 3m.

Stop criterion. While adjusting the observations into the model, that parameters of the model are sought for that minimize the distance of the observations to the model space with respect to the variance-covariance metric. This implies that for a least squares solution of a model adjustment, the residuals $\hat{e}$ of the observations are perpendicular to the model, that is $\hat{e} \perp A \cdot \hat{x}$. A good reliable criterion, (Teunissen, 1990), for a linearized adjustment is therefore

$$\|(x^{k+1} - x^k)^\top \cdot Q_{x_k}^{-1} \cdot (x^{k+1} - x^k)\| \quad < \epsilon, \qquad (10)$$

where x^k denotes the values of the model parameters after the i-th iteration, and Q_{x_k} it's VC-matrix. The threshold value ϵ should be chosen small enough. Here, a value of $\epsilon = 1 \cdot 10^{-8}$ is used.

2.2 Deformation analysis.

The deformation analysis method can be separated into two parts. The first part consists of comparing the tunnel data in some epoch with an idealized model, i.e. a cylinder. The second part is a method to test whether (artificial) deformation occurred between two epochs of tunnel measurements.

For comparing the actual tunnel data to an idealized model, the data is fit to the model and the resulting residuals are analyzed. Deformation between two epochs is determined in a number of steps:
• Transform tunnel data of both epochs into a suited, in our case cylindrical, coordinate system, in such a way that all deformation occurs along one *range* coordinate.
• Interpolate data from both epochs to a regular grid in the two *domain* coordinates in this coordinate system
• Test whether the differences in range coordinate at a grid point between the two epochs is relevant given the propagated accuracy of the interpolated points.

Cylindrical coordinates. Before the start of the deformation analysis all data was registered to a common xyz Cartesian coordinate system. As deformations of the tunnel wall are looked for, a coordinate system is required that allows expressing the location of a point on the tunnel wall by two domain coordinates, and the 'signal' at that location as a third, range, coordinate.

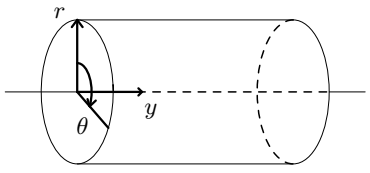

Figure 2. Cylindrical (y, θ, r) coordinates.

This is achieved by the coordinate system of Fig. 2. Here, 'y' denotes the distance along the tunnel axis, 'θ' the angle in a plane perpendicular to the tunnel axis, and 'r' the distance in this plane to the tunnel axis. Now, after fixing the axes origins, any location on the tunnel wall can be expressed as a pair (y_0, θ_0), while the 'signal' at that location is given by the third coordinate, the distance r_0 to the tunnel axis. The coordinate transformation

$$y \;=\; y, \qquad \theta \;=\; \arctan z/x, \qquad r \;=\; \sqrt{x^2 + z^2} \qquad (11)$$

transforms Cartesian xyz coordinates into cylindrical coordinates with cylinder axis y.

Interpolation of the distance to the tunnel axis. Using this coordinate system a grid on the tunnel wall is defined in terms of the (y, θ) coordinates. Within a grid cell

$$[y_0 - \Delta y, y_0 + \Delta y] \times [\theta_0 - \Delta\theta, \theta_0 + \Delta\theta],$$

the tunnel wall is assumed to be flat. A value $\hat{r}_0$ at location (y_0, θ_0) is obtained by averaging all observations within the grid cell. Except for the value $\hat{r}_0$ itself also its precision $\sigma^2_{\hat{r}}$ is obtained as, (Teunissen, 2000a),

$$\sigma^2_{\hat{r}} \quad = \quad (A_G^\top \cdot Q_y^{-1} \cdot A_G)^{-1}, \qquad (12)$$

with $Q_y \;=\; \sigma_{\text{point}} \cdot I_m$ the VC-matrix of the measurements, and $\underset{m\times 1}{A_G} = (1, 1, \ldots, 1)^\top$ the model matrix that reflects that the average of all m observations was taken. It should be noted that strictly speaking not an interpolation, which is always less precise than the underlying observations, but an adjustment is performed.

Testing for deformation. Once the difference $\hat{r}_1 - \hat{r}_2$ in distance to the cylinder axis is determined between two epochs 1 and 2 for each grid point, it remains to be found out if such a difference is just due to measurement noise, or if a real deformation took place. This can be tested for by a stability test, (Teunissen, 2000b). In a stability test the A-model $A_S = (1, 1)^\top$ models the situation of no deformation, which implies that $\hat{r}_1$ and $\hat{r}_2$ are two observations of the same attribute r_S. Solving the system

$$E\{\begin{pmatrix} \underline{r}_1 \\ \underline{r}_2 \end{pmatrix}\} = A_S \cdot r_S; \qquad Q_y = \begin{pmatrix} \sigma^2_{\hat{r}_1} & 0 \\ 0 & \sigma^2_{\hat{r}_2} \end{pmatrix}, \qquad (13)$$

gives the adjusted, common distance

$$\hat{r}_S = (A_S^\top \cdot Q_y^{-1} \cdot A)^{-1} \cdot A^\top \cdot Q_y^{-1} \cdot \begin{pmatrix} \underline{r}_1 \\ \underline{r}_2 \end{pmatrix}, \qquad (14)$$

together with the vector $\underline{\hat{e}}$ of epoch-wise residuals:

$$\underline{\hat{e}} = \begin{pmatrix} \underline{r}_1 \\ \underline{r}_2 \end{pmatrix} - \begin{pmatrix} \hat{r}_S \\ \hat{r}_S \end{pmatrix}. \qquad (15)$$

It remains to test the zero hypothesis H_0, that states that the size of the remaining residuals is acceptable, given the accuracy of the observations and the assumption that no deformation took place. The test quantity $\underline{T}_q = \underline{\hat{e}}^\top \cdot Q_y^{-1} \cdot \underline{\hat{e}}$, with $q = m - n = 1$ the degrees of freedom, has, under the zero hypothesis, a chi-square distribution:

$$H_0 : \underline{T}_q \sim \chi^2(q, 0) \qquad (16)$$

The test quantity is tested against a critical value κ_α, where α denotes the reliability level of the test. If $T_q > k_\alpha$, the test states that deformation took place.

In this testing framework easily other tests can be used instead of the stability test (Teunissen, 2000b). If, e.g., several epochs of data are available, one can decide to actually model a deformation and test whether this model effectively describes the deformation signal as found in the measurements. It is also common practice to test whether an extension of a model by an extra parameter gives a relevant improvement of the model fit.

Figure 3. Left: photograph of the 2e Heinenoordtunnel. Right: laser scan, colored by intensity, from red to blue. Clearly visible is the low reflectivity of the asphalt in contrast to the high reflectivity of the road markers.

3. PROCESSING THE TUNNEL DATA

3.1 Measurement setup.

During the measurement project in the 2^{nd} Heinenoordtunnel, two times a length of 100m tunnel were scanned. This scanning had to be done during one night due to traffic regulations. Therefore a careful measurement setup was designed before the actual scanning took place. In order to reduce a possible influence of systematic errors scanner positions were approximately the same in both epochs. Distances between scanner positions were not equal but varied from 5m to 25m in order to have a dataset with different measurement distances to the tunnel surface. Four subsets of the data will be analyzed. Subset 1 has an average along-tunnel-axis distance of 5m and is covered by one scan. Subset 2 is immediately around a scanner position. Subset 3 is in the middle of two scan positions with a distance of 12m to the scanner positions on either side, and subset 4 has a distance of 15m to the used scanner positions. Each subset has a width of 4.5m.

Choice of scanner As mentioned in the introduction, phase scanners surpass pulse round trip time scanners in speed and point density, which is in the case of limited access to the object of importance, at the cost of lower maximum range. However, the elongated geometry of a tunnel leads to low incidence angles and deterioration in precision for long ranges anyway. The setup of the scanner positions was such that the maximal distance of an object point to the scanner was no more than 15m. The choice for the Leica HDS4500 was based on the availability of the instrument. The maximum used range was set to 20m, and given the tunnel diameter of 7.6m this leads to an incidence angle as low as 10°. The data collection of the 2^{nd} Heinenoordtunnel showed that in 20min about 40m of tunnel can be scanned.

Artificial deformations After having scanned the tunnel for the first time, artificial deformations were put against the tunnel wall, see Fig. 4. The deformations consist of a foam plate of 30×40×3cm, of a thin wooden plank of 10cm wide and 2cm thick, Fig. 4, left, and of several plastic caps and lids of a maximal diameter of 13cm, Fig. 4, right.

3.2 Data quality description.

Two times, a length of 100m tunnel is scanned, see also Fig. 3. The time between the two measurements is only a few hours, during which the artificial deformations were placed. The data from the different scan positions and two different epochs were registered using the program Cyclone (Leica Geosystems, 2005).

Figure 4. Artificial deformations placed against the tunnel wall.

According to the software, the registration accuracy is global and equals σ_R = 3mm. The accuracy of a single measurement equals σ_M = 7mm, as stated by the HDS4500 specifications (Leica Geosystems, 2006). By combining σ_R and σ_M via

$$\sigma_P^2 = \sigma_M^2 + \sigma_R^2, \tag{17}$$

a single point precision σ_P = 7.6mm is obtained after registration.

After registration, data clearly not belonging to the cylindrical part of the tunnel surface was manually removed, like data from the road surface, see Fig. 3. This step is a source of possible errors and should be improved in future. Especially points reflected on the joints between the concrete segments and by the grip holes within the segments were only partly removed. These grip holes are used by the tunnel building machine to place the concrete segments. It is however not trivial to remove grip hole data, as the grip holes increase very smoothly in depth and are smoothly joined to the actual segment surface.

After registration and filtering 2× four subsets of data of 4.5m tunnel length, each covering three neighboring tunnel rings of 1.5m each, were analyzed. A single subset consist of 1 million data points on average.

3.3 Results of the cylinder fitting.

Using 1% of the available data, i.e. using $\pm 10\ 000$ points per subset, the cylinder parameters $\mathbf{p}$, $\mathbf{a}$ and r were estimated in a linearized least squares adjustment, as described above, for all four subsets. Thinning out was performed by a function implemented in Cyclone. In all cases, the stop criterion was met after about 5 iteration steps. The results for the cylinder radius r for the data of the first epoch are given in Table 1.

	subset 1	*subset 2*	*subset 3*	*subset 4*
Initial r	3.7587	3.7577	3.7663	3.7649
One iteration r	3.7825	3.7885	3.7945	3.7956
# iterations	5	4	5	4
Final r	3.7952	3.7943	3.8056	3.8046
Final σ_r	0.00016	-	-	-

Table 1. Estimated cylinder parameters in meter.

In all cases the estimated radius differs only 5mm with the designed radius. Except for the actual parameters itself, the adjustment procedure gives the variance-covariance matrix $Q_{\hat{x}}$ of the estimated parameter vector $\hat{x}$ as well. Table 1 gives as an example the value of the radius standard deviation as $\sigma_r = 0.16$mm. This value seems optimistic however. It is expected that the error description will be more realistic if the cylinder constraints, as introduced in Equation 8, will be incorporated using a constrained adjustment by means of Lagrange multipliers.

For this adjustment all points on the tunnel wall had an equal observation accuracy of $\sigma_P = \pm 7.6$mm. This part of the procedure should be improved in future as this error model is too much simplified: points far away from the scanner have a relative bad incidence angle. When this is encoded in the VC-matrix, these observations will get lower weights. This may have the drawback that mainly the points near the scanner are used in determining the cylinder parameters, although it is numerically difficult to fit an elongated cylinder through a small strip of observations.

3.4 Deviations from the tunnel model

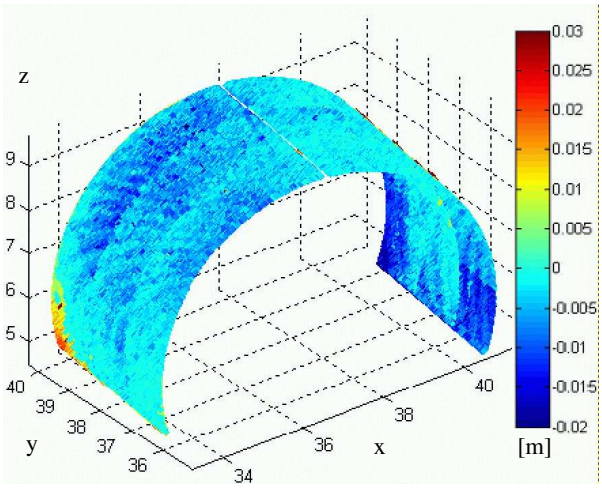

Figure 5. Residuals in m after fitting of a cylindrical model to the tunnel data. In each single segment gripper holes can be detected. Some offset seems to occur in the segments on the bottom right while the segment in the bottom left corner looks damaged.

In Fig. 5 the residuals of the scan points after adjustment to a cylindrical model are shown. These are the residuals from Subset 3 in the first epoch. Clearly the three different tunnel rings are visible, but it is not easy to distinguish the individual segments, cf. Fig. 3, except for the dark blue segment in the bottom right of the figure. On the other hand, larger residuals of upto 3cm due to the presence of gripper holes are present at regular distance in the residual image. On the bottom left, near coordinates (40.5, 34.0), a strongly deviating segment is visible. Probably this segment was placed in a bad way during construction of the tunnel.

Results from the other subsets are similar: different rings are visible, while several local deviations from the adjusted tunnel model are clearly visible. For Subset 4, the deviation pattern is more diffuse, see Fig. 6. As deviations are here more global it is not clear if they are caused by actual deformation. Especially the pressure of the soil above cannot be used for explanation as the deformation pattern would have to be exactly the other way around. A possible explanation for the periodicity of 360 degrees is an eccentricity error due to a (unexpected) biased estimation of the cylinder position. Another error source could be registration errors considering that the point density is lowest in that area of either scan.

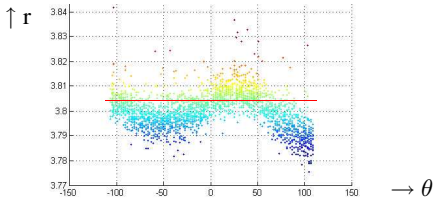

Figure 6. Scatterplot of (θ, r) values of Subset 4 residuals after adjustment in a cylinder model. The red line indicates the tunnel radius as found by the fitting procedure.

3.5 Deformation between two epochs.

To test for changes between the two measurement epochs, 1 % of the data from both epochs was interpolated to a regular grid of 15 $\times$ 15cm along the tunnel wall. Interpolation is in cylindrical coordinates w.r.t. the tunnel model as estimated from the data from the first epoch. Using a level of significance of $\alpha = .05$, all grid points from all four subsets were tested for stability in the radius direction r. In Fig. 7 the test quantities T_q are given for subset 2.

It turns out that for the second subset 3.0% of the grid points are rejected by the stability test. Large test quantities, clearly indicating deformation, can be found at location A, were the foam plate was placed between the two epochs and to a smaller extend at location B, the position of the wooden plank. Plastic lids and caps were placed near location C, but these were only partly found, due to the large grid size of 15cm in comparison to the small maximal diameter of 13cm of the lids and caps.

Except for the placed, artificial deformations, the stability test found instabilities at several other grid points. It appears that many 'instabilities' occur adjacent to missing grid points. These type I errors are caused by the grip holes in the concrete segments. Even a small registration error can cause relative high differences between corresponding grid points in the two epochs. From Fig. 5 it is concluded, as expected, that near the grip holes larger residuals with the cylindrical model occur. If two grip holes do not exactly match, the larger residuals will contribute to partly different grid points in the two epochs, thereby causing high test statistics. The occurrence of missing adjacent grid points is either caused by the preprocessing step, where strongly deviating points were manually removed or by scan shadows from the grid holes, compare also Fig. 3. Of course, the choice of scanner position, which was not strictly the same between the two epoches, has an influence on this procedure. Especially for surfaces where the simple local model does not fit to the real situation, i.e. around the grip holes, the inclusion or neglection of one point has a strong impact on the estimated parameter(s). With different scanner positions it naturally happens that the number of points measured in the grip holes varies between the epochs.

4. CONCLUSIONS AND FUTURE WORK

This report describes one of the first investigations of the possibilities of deformation analysis with laser scanning. It shows that

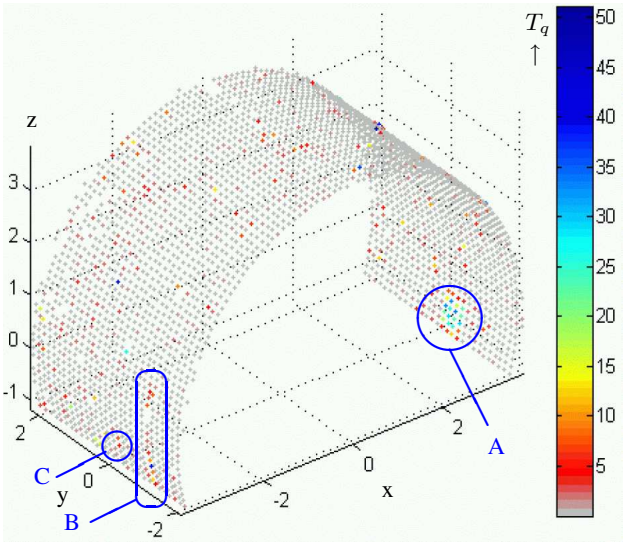

Figure 7. Results of the stability test. Test quantity per grid point. The larger artificial deformations A and B (the foam and wooden planks) were found back by the testing procedure. Moreover, the procedure finds several other 'deformations' near the grip holes, but this are errors caused by registration mismatches.

good possibilities exist for the application of geodetic deformation analysis on terrestrial laser scanning data. The method and computational program developed are able to detect deformations in laser scanning data. Nevertheless, method and software have to be developed further before extensive used in practice. Laser scanning can definitely be used for making as-built visualizations and the determination of the tunnel deformations with respect to the design. This research shows that laser scanning is a good supplement of the present measurement techniques that are used by the municipality of Rotterdam.

From the performed deformation analysis it appears that the 2^{nd} Heinenoordtunnel has not become oval. It does, however, show systematic deviations from the design model. The rings of the tunnel are tilted with respect to the estimated cylinder model which was adjusted over three rings. While each ring apparently fits well to a cylinder model, the axes of the individual rings do not coincide with one line. These results were obtained by visual analysis of the residual pattern. It is advisable to further investigate the scan data for the presence of such patterns.

Application of the deformation analysis on the scan data of the 2^{nd} Heinenoordtunnel shows that all deformations larger than 15mm in radial direction are being detected by the stability test. It remains to be studied if using a higher point density allows reducing this value further, or if registration errors and correlation within the data hinders improving the results. It is expected that reduction of the grid size, coupled with analyzing of more scan points will decrease the smallest deformations that can be detected by this method.

This analysis however also reveals two problems. Firstly, sometimes points are incorrectly marked as being deformed. One of the reasons for this is inaccuracies in the registration of the scans. Secondly, the used stochastic model is not an appropriate description of reality. The measurement accuracy of the phase-based scanner is not constant but it decreases with distance.

It is desired to investigate the registration methods that are implemented in the processing software of the scanners, in order to know how the scans are registered and how accurate this is done. Besides that, the results of the deformation analysis will be improved when the behavior of the scanner accuracy is known.

However, on the methodology side gain can be made as well. The current testing method only takes grid point deformation into account, although there is clearly spatial correlation in the deformation near locations A and B in Fig. 7. Therefore it is recommended to extend the testing procedure by a spatial component.

It can be argued that it is not necessary to actually model and fit the cylindrical tunnel model to the data for detecting deformation between the epochs: when considering at least two epochs, the tunnel cancels out when considering deviations. Here the modeling was done anyway, because study of deviations from the tunnel model was one of the project targets. Additionally a fitted model helps in laying out a grid for analysis.

All approaches considered have in common that they will benefit from an improved stochastic model. The registration error is now taken uniformly, although the error is much stronger away from the tie points(/elements), especially for scans of elongated scenes, like tunnels. Also the scan point error is taken uniformly, although it is already known that this error at least varies with intensity and incidence angle. Fig. 3 shows that these two parameters are both relevant in this setting.

ACKNOWLEDGMENTS

The authors would like to thank Theo Koster, Lennard Huisman and Frank Kenselaar from Gemeentewerken Rotterdam for the fruitful cooperation. Moreover Peter Teunissen and the reviewers are thanked for useful remarks.

REFERENCES

Blug, A., Baulig, C., Wölfelschneider, H., and Höfler, H., 2005. Novel geometry for a high speed outdoor laser scanning system. In *Proceedings 7th conference on optical 3-D Measurement Techniques*, Vienna.

Dibit, Accessed: July 2006. http://www.dibit-scanner.at/

Kontogianni, V., and Stiros, S., 2003. Tunnel monitoring during the excavation phase: 3-D kinematic analysis based on geodetic data. Proc. of the 11th FIG Symposium on Deformation Measurements, Santorini, Greece.

Lemmens, M., 2004. Product survey 3d lasermapping. *GIM International* 18(12), 44–47.

Lukács, G., Marshall, A., and Martin, R., 1997. Geometric least-squares fitting of spheres, cylinders, cones, and tori. In *RECCAD, Deliverable Document 2 and 3, COPERNICUS project, no. 1068, Geom. Modelling Lab. Studies/1997/5*, Computer and Automation Research Inst. Budapest.

Leica Geosystems, Accessed: March 2006. HDS4500 specifications. http://www.leica-geosystems.com/hds/en/HDS4500_25m_and_53m.pdf.

Leica Geosystems, 2000-2005. HDS LLC Cyclone. version 5.3.

Paar, G., Bauer, A., and Kontrus, H., 2005. Texture-Based Fusion between Laser Scanner and Camera for Tunnel Surface Documentation. Proc. of 7th Int. Conf. on Optical 3-D Measurement Techniques, Vienna, Austria.

POB, Accessed: March 23, 2006. 2005 3d laser scanner hardware & software surveys. http://www.pobonline.com/POB/Protected/Files/PDF/-POB0105-LaserScanningSurvey.pdf.

Schulz, T., and Ingensand, H., 2004. Terrestrial Laser Scanning - Investigations and Applications for High Precision Scanning. Proceedings of the 'FIG Working Week - The Olympic Spirit in Surveying', Athens, Greece.

Teunissen, P. J. G., 1990. Nonlinear least squares. *Manuscripta Geodeaetica* 15, 137–150.

Teunissen, P. J. G., 2000a. *Adjustment theory*. Delft: Delft University Press.

Teunissen, P. J. G., 2000b. *Testing theory*. Delft: Delft University Press.

Tsakiri, M., Lichti, D., and Pfeifer, N., 2006. Terrestrial laser scanning for deformation monitoring. In *Proceedings of 12th FIG symposium on deformation measurements and 3rd IAG symposium on geodesy for geotechnical and structural engineering*, Baden, Austria.